Geophysical Prospecting, 1998, **46**, 141–151

iSPI™ – the improved source parameter imaging method[1]

Richard S. Smith,[2] Jeffrey B. Thurston,[2] Ting-Fan Dai[3] and Ian N. MacLeod[3]

Abstract

Interpretation of an anomalous magnetic response involves determining the parameters that characterize the source of the anomaly. The depth to the top of the structure is a parameter that is commonly sought, and the Source Parameter Imaging™ (SPI™) method is one way of determining this depth estimate. One advantage of the SPI method is that the depths can be displayed on an image. Typically there can be one image for an assumed contact (fault) model and another image for an assumed dipping thin sheet (dike) model. The depth estimate obtained will depend on the model assumed.

An improvement to the source parameter imaging method extends the method to horizontal cylinders and at the same time allows the most appropriate model to be determined automatically. This model can be displayed on an image and the correct depth estimate for each anomaly can also be determined. The depth estimates can therefore be summarized on one map independent of an assumed model.

The images generated from synthetic and field data show that the improved SPI method makes the task of interpreting magnetic data significantly easier.

Introduction

A large number of automatic methods exists for interpreting magnetic data. These methods can be applied to profile data (Hartman, Tesky and Friedberg 1971; Naudy 1971; Nabighian 1972; Jain 1976; Thompson 1982; Atchuta Rao, Ram Babu and Sanker Narayan 1981) or grid data (Reid *et al.* 1990; Roest, Verhoef and Pilkington 1992; MacLeod, Jones and Dai 1993; Hsu, Sibuet and Shyu 1996). All the techniques assume a certain model and then determine the parameters which characterize the source subject.

We have experience of in-house work by the Compagnie Générale de Géophysique (on the Naudy technique) and by Jain (on the Werner deconvolution method). Each of these methods has a number of rules of thumb for determining the most appropriate

[1] Received January 1997, revision accepted November 1997.

[2] Geoterrex-Dighem, a division of CGG Canada Ltd, 2060 Walkley Road, Ottawa, Ontario, Canada, K1G 3P5.

[3] Geosoft Inc., 8th floor, 85 Richmond St West, Toronto, Ontario, Canada, M5H 2C9.

model. No doubt similar unreported work has been undertaken at other centres. Unfortunately, the rules we are aware of are empirical and require a great deal of experience to apply with confidence. Hence, they are not easily adapted to automatic application. There has been some work on a variation of the Euler method (Neil 1990; Neil, Whaler and Reid 1991) which automatically outputs the model (the Euler 'structural index') along with the position and depth. Reid (1995), in reviewing this aspect of the Euler deconvolution method, concluded that 'work remains to develop a reliable method of estimating structural index'.

We describe an improvement to the source parameter imaging method^{TM} (SPI^{TM}). The output from the SPI method (Thurston and Smith 1997) is an image from which the depth can be determined. (If we assume no remanent magnetization, the dip and susceptibility contrast can also be estimated.) Like the other methods, a particular source model is assumed (either a sloping contact or a dipping thin sheet). The improved SPI (iSPI^{TM}) method analyses the properties of the analytic-signal response and the second-derivative analytic-signal response. From this analysis, the appropriate model can be determined, and we can obtain an estimate of the depth that is independent of any assumptions about the model. Like the SPI method, the improved SPI method is applicable to contacts and thin sheets. In addition, the horizontal cylinder model has been incorporated.

This means that the process of interpreting magnetic data is made significantly simpler. A stated goal of the SPI method (Thurston and Smith 1997) is that the resulting images can be easily interpreted by someone who is an expert in the local geology. The improvement to the method we describe brings us a significant step closer to that goal.

Methodology

Definitions

The SPI method (Thurston and Smith 1997) estimates the depth from the local wavenumber of the analytic signal. The analytic signal $A_1(x,z)$ is defined by Nabighian (1972) as

$$A_1(x,z) = \frac{\partial M(x,z)}{\partial x} - \mathrm{j}\frac{\partial M(x,z)}{\partial z}, \tag{1}$$

where $M(x,z)$ is the magnitude of the anomalous total magnetic field, j is the imaginary number, and z and x are Cartesian coordinates for the vertical direction and the horizontal direction perpendicular to strike, respectively. Nabighian (1972) shows that the horizontal and vertical derivatives comprising the real and imaginary parts of the 2D analytic signal are related as follows:

$$\frac{\partial M(x,z)}{\partial x} \Leftrightarrow -\frac{\partial M(x,z)}{\partial z}, \tag{2}$$

where $\Leftrightarrow$ denotes a Hilbert transform pair. The local wavenumber κ_1 is defined by

Thurston and Smith (1997) to be

$$\kappa_1 = \frac{\partial}{\partial x}\tan^{-1}\left[\frac{\partial M}{\partial z}\Big/\frac{\partial M}{\partial x}\right]. \tag{3}$$

We use the concept of an analytic signal comprising second-order derivatives of the total field, in a manner similar to that used by Hsu *et al.* (1996). The analytic signal defined by Nabighian (1972) uses the Hilbert transform pair in (2). The Hilbert transform and the vertical-derivative operators are linear, so the vertical derivative of (2) will give the Hilbert transform pair,

$$\frac{\partial^2 M(x,z)}{\partial z\,\partial x} \Leftrightarrow -\frac{\partial^2 M(x,z)}{\partial^2 z}. \tag{4}$$

This enables us to define an analytic signal based on second-order derivatives, $A_2(x,z)$, where

$$A_2(x,z) = \frac{\partial^2 M(x,z)}{\partial z\,\partial x} - \mathrm{j}\frac{\partial^2 M(x,z)}{\partial^2 z}. \tag{5}$$

This gives rise to a second-order local wavenumber κ_2, where

$$\kappa_2 = \frac{\partial}{\partial x}\tan^{-1}\left[\frac{\partial^2 M}{\partial^2 z}\Big/\frac{\partial^2 M}{\partial z\,\partial x}\right]. \tag{6}$$

The first- and second-order local wavenumbers are used to determine the most appropriate model and a depth estimate independent of any assumptions about a model.

Magnetic anomalies

Nabighian (1972) gives the expressions for the vertical and horizontal gradients of a sloping contact model as

$$\frac{\partial M}{\partial x} = 2KFc\sin d\,\frac{h_c\cos(2I-d-90)+x\sin(2I-d-90)}{h_c^2+x^2}, \tag{7}$$

$$\frac{\partial M}{\partial z} = 2KFc\sin d\,\frac{x\cos(2I-d-90)-h_c\sin(2I-d-90)}{h_c^2+x^2}, \tag{8}$$

where K is the susceptibility contrast at the contact, F is the magnitude of the earth's magnetic field (the inducing field), $c = 1-\cos^2 i\sin^2\alpha$, α is the angle between the positive x-axis and magnetic north, i is the ambient-field inclination, $\tan I = \tan i/\cos\alpha$, d is the dip (measured from the positive x-axis), h_c is the depth to the top of the contact and all trigonometric arguments are in degrees. The coordinate system has been defined such that the origin of the profile line ($x = 0$) is directly over the edge.

The expression for the magnetic-field anomaly due to a dipping thin sheet is

$$M(x,z) = 2KFcw\,\frac{h_\mathrm{t}\sin(2I-d) - x\cos(2I-d)}{h_\mathrm{t}^2 + x^2} \tag{9}$$

(Reford 1964), where w is the thickness and h_t the depth to the top of the thin sheet.

The expression for the magnetic-field anomaly due to a long horizontal cylinder is

$$M(x,z) = 2KFS\frac{\sin i}{\sin I}\,\frac{(h_\mathrm{h}^2 - x^2)\cos(2I-180) + 2xh_\mathrm{h}\sin(2I-180)}{(h_\mathrm{h}^2 + x^2)^2} \tag{10}$$

(Murthy and Mishra 1980), where S is the cross-sectional area and h_h is the depth to the centre of the horizontal cylinder.

First- and second-order local wavenumbers

Substituting (7), (8), (9) and (10) into the expressions for the first- and second-order local wavenumbers, we obtain, after some simplification, a remarkable result:

$$\kappa_1 = \frac{(n_\mathrm{k}+1)h_\mathrm{k}}{h_\mathrm{k}^2 + x^2} \tag{11}$$

and

$$\kappa_2 = \frac{(n_\mathrm{k}+2)h_\mathrm{k}}{h_\mathrm{k}^2 + x^2}, \tag{12}$$

where n_k is the SPI structural index (subscript k = c, t or h), and $n_\mathrm{c} = 0$, $n_\mathrm{t} = 1$ and $n_\mathrm{h} = 2$ for the contact, thin sheet and horizontal cylinder models, respectively. We have defined the SPI structural index so that for the thin sheet and contact models, the numerical values are identical to the numerical values of the Euler structural index (as defined by Reid *et al.* (1990)). From (11) and (12), it is evident that the first- and second-order local wavenumbers are independent of the susceptibility contrast, the dip of the source and the inclination, declination, and strength of the earth's magnetic field. The significance of this result can be better understood by looking at the first- and second-order local wavenumbers for each model as listed in Table 1. The local wavenumbers κ_1 and κ_2 have an identical functional form for all three of the above two-dimensional models. In each case they are symmetric about $x = 0$, and take on their maximum value at this position. The position $x = 0$ defines the source location, so this can be determined easily from either local wavenumber. The only difference between $_1$ and κ_2 is a change in the amplitude factor, which is related to the structural index n_k. The consequences of this are as follows:

1 A model-independent local wavenumber can be calculated from $(\kappa_2 - \kappa_1)$. The peak value of this function (at $x = 0$) is always $1/h_\mathrm{k}$, i.e. it has the same functional form for all three models. The model-independent depth can thus be estimated as the inverse of this peak value (second last row of Table 1).

Table 1. The first- and second-order local wavenumbers for three different models. Combinations of the first- and second-order local wavenumbers give the model-independent depth estimate and the SPI structural index.

	Contact	Thin sheet	Horizontal cylinder
κ_1	$h_c/({h_c}^2+x^2)$	$2\ h_t/({h_t}^2+x^2)$	$3\ h_h/({h_h}^2+x^2)$
κ_2	$2\ h_c/({h_c}^2+x^2)$	$3\ h_t/({h_t}^2+x^2)$	$4\ h_h/({h_h}^2+x^2)$
$\kappa_2-\kappa_1$	$h_c/({h_c}^2+x^2)$	$h_t/({h_t}^2+x^2)$	$h_h/({h_h}^2+x^2)$
Model-independent depth $\{1/(\kappa_2-\kappa_1)\}\mid_{x=0}$	h_c	h_t	h_h
SPI structural index $\kappa_1/(\kappa_2-\kappa_1)-1=n_k$	0	1	2

2 The quantity $(\kappa_1/(\kappa_2-\kappa_1)-1)$ gives the structural index for each model (last row of Table 1).

The contact, thin sheet and horizontal cylinder are all two-dimensional models (infinite strike extent), so it is an implicit assumption of the SPI method that the geology is two-dimensional. If the body is two-dimensional and there is no interference from nearby bodies, the depth estimate will be reasonable and the structural index should be constant over the entire area for which the response is anomalous.

Synthetic examples

Figure 1(a) shows profiles of the first- and second-order local wavenumbers for a dipping contact model buried 100 m below the traverse. The model-independent local wavenumber is shown in Fig. 1(b). The peak value is 0.01 m^{-1}, and the depth is the inverse of this value. The SPI structural index is shown in Fig. 1(c); at all positions it is equal to 0.

The method has been extended to gridded data by estimating the strike direction at each gridpoint. We calculate the vertical derivatives in the frequency domain and the horizontal derivatives are computed in the direction perpendicular to strike using the least-squares method of Thurston and Brown (1994). The same methodology was used by Thurston and Smith (1997) when implementing the SPI method for gridded magnetic data.

The application of the method to synthetic gridded data is shown on Fig. 2. Figure 2(a) shows a grid of total-field magnetic data containing the anomalies from two bodies, both of which are buried at 0.5 km depth and both are square in plan view. The body to the south-west is thin, and the north-east body is effectively infinite in depth extent. At the centre of the edges, the magnetic field contours are roughly parallel, so the bodies are approximately two-dimensional. At the centre of the edges, the thick and thin bodies therefore approximate a contact and a flat-lying thin sheet, respectively. As expected, the peak of the first-order local wavenumber (Fig. 2b) over the edges of the thin sheet is approximately twice the peak over the contact. If the inverse of the

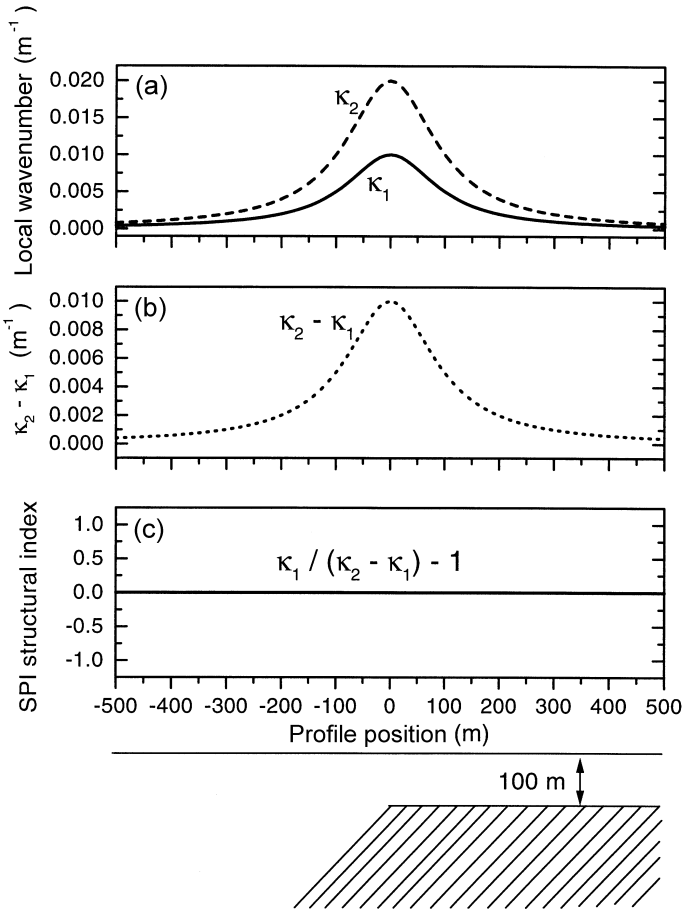

Figure 1. The dipping contact model. (a) The first- and second-order local wavenumber (κ_1 and κ_2) for the model shown at the bottom of the figure. The dip is 135°, the depth to the top is 100 m, the ambient field strength is 60 000 nT, the susceptibility contrast is 0.01 SI, and the declination is 0°. (b) The model-independent local wavenumber ($\kappa_2 - \kappa_1$). (c) The SPI structural index $\kappa_1/(\kappa_2 - \kappa_1) - 1$. Similar plots apply for the dipping thin sheet and the long horizontal cylinder model, except that the amplitudes and hence the values of the SPI structural index differ.

first-order local wavenumber is used to estimate the depth, the correct depth will only be obtained where the structure approximates a contact (at the centre of the edges of the north-east body).

The model-independent depth estimate is shown in Fig. 2(c). In this case, roughly the same depth is obtained for both bodies.

The SPI structural index is shown in Fig. 2(d). At the centre of the edges, where the data are approximately two-dimensional, the structural index parameter is close to 0 for the contact, and close to 1 for the thin sheet. In source-free regions, the structural

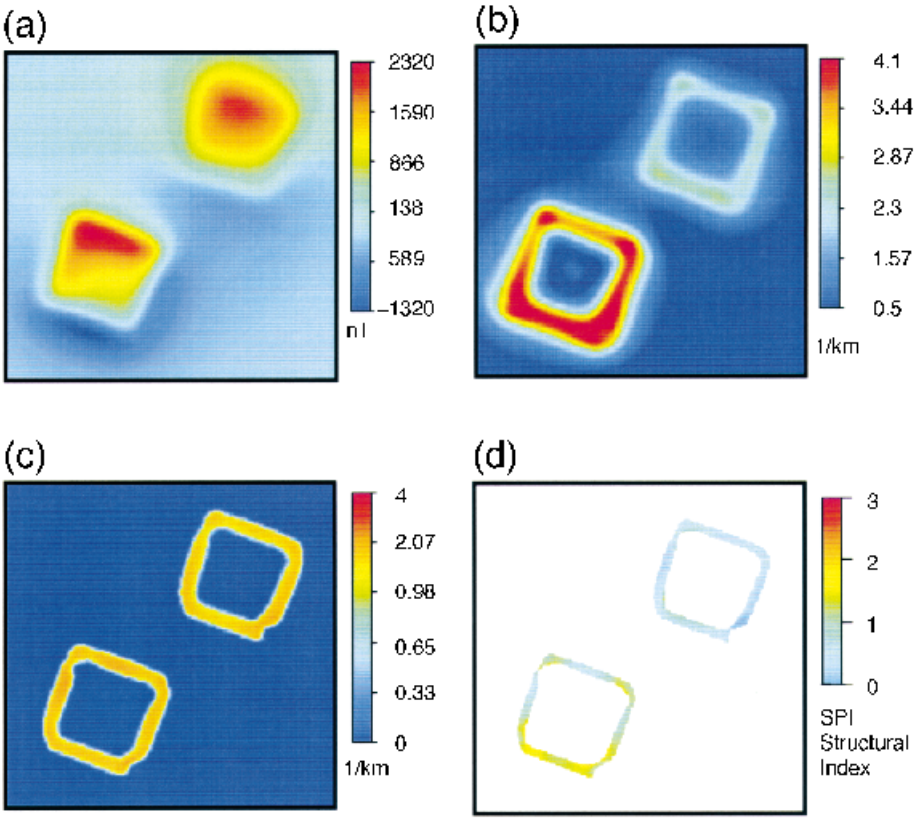

Figure 2. The synthetic example. (a) The total-field anomaly of two bodies. North is to the top of the page. One body (to the north-east) is a parallelepiped model 2500 m by 2500 m, with a depth to top of 500 m, and a depth to bottom of 20 km. The sides of the model are vertical, but are orientated 20° to the east of grid and magnetic north. In SI units, the susceptibility contrast at the edge is 0.13. The other body (to the south-west) is the same, except that the thickness is 550 m and the susceptibility contrast is 2.5 SI units. The earth's magnetic field has an inclination of – 61° (southern hemisphere), a declination of zero, and a field strength of 56 000 nT. The map area shown is 8.5 km square. (b) The first-order local wavenumber of the total magnetic field. Note that the peaks over the thin sheet are twice as large as the peaks over the body of infinite depth extent. (c) The model-independent depth – the same depth estimate is obtained for both models. (d) The SPI structural index. Where the structural index is close to 0, the body is effectively a contact, and where it is close to 1, it is effectively a thin sheet.

index calculation becomes unstable as κ_1 and κ_2 approach zero. In these regions, we have made the image white.

Field example

As a field example, we have chosen a single anomaly in the non-exclusive data set

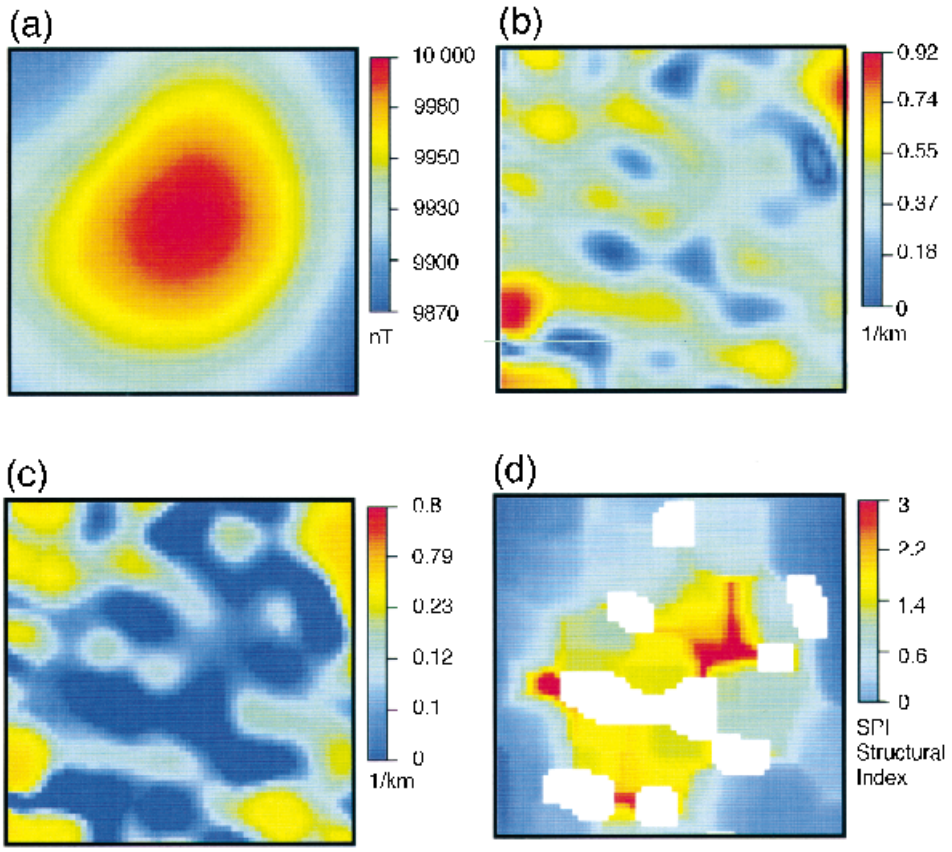

Figure 3. A field example. (a) The total-field anomaly for a single feature on a larger non-exclusive survey in the Peace River area near the border of Alberta and British Columbia (Canada). The survey was flown at a constant barometric altitude. The image is 15 km by 15 km and north is to the top of the page. (b) The first-order local wavenumber for the area. At the peak positions, the inverse of this quantity will give the depth to a contact. (c) The model-independent wavenumber; the inverse of this quantity at the peak position will give the correct depth for a contact, thin sheet or a horizontal cylinder. (d) The SPI structural index. At the edges of the strong magnetic feature, the index is close to 1, implying that the source associated with the strong magnetic feature is a thin sheet.

discussed by Thurston and Smith (1997). The total-field anomaly (Fig. 3a) is near the Peace River at the Alberta/British Columbia border. Here the basement is known from drilling information to be 4.7 km below the elevation of the survey aircraft. The second-order local wavenumber is shown in Fig. 3(b) and the model-independent wavenumber in Fig. 3(c). The inverse of the model-independent wavenumber at the peaks near the edge of the large anomaly are about $0.2\,\mathrm{km}^{-1}$, giving depths of about 5 km, which is just below the top of the sediment/basement interface. The depths on the north and south edges are comparable, indicating that the top of the body is relatively

flat. All the features on the model-independent wavenumber image run east of north-east, implying that the structures in the basement have this principal direction. Interestingly, this direction is not evident from the total-field map (Fig. 3a). The form of the body is evident from the SPI structural index image, which shows that the structural index is close to 1 on the southern edge of the feature of interest. This implies that the body is a horizontal thin sheet. On the north edge of the feature the structural index is greater than 1, and this occurs where the body is least two-dimensional. The white areas are where the derivatives used to estimate the local wavenumbers are so small that the SPI structural index cannot be estimated reliably. The model-independent local wavenumber has been set to zero in the same areas.

Away from the main feature, the model-independent wavenumber shows depths of less than 4 km and structural indices of less than 1. This implies that there are contact-like features (faults) in the overlying sediments. They follow the east–north-east trend and may be associated with similarly trending features in the basement which have no magnetic signature or a magnetic signature which has been swamped by the shallower features. The fact that there is little manifestation of these features in the total field implies that the susceptibility contrast is not great.

Discussion

The method is sensitive to random noise. Our experience is that the method can work well when the measured total-field data are of high quality, and these data have been carefully levelled and processed. It is also important to ensure that noise is not generated in the process of calculating the higher-order vertical and horizontal derivatives. Careful filtering of these data ensures good estimates of the local wavenumbers and hence the depth and structural index.

The mathematical form of the first- and second-order local wavenumbers is amazingly simple. Furthermore, the only difference between wavenumbers of different order and wavenumbers of different models is that the amplitude factor (structural index) varies. The systematic variation of structural index suggests that the results we obtained for the specific cases presented could be generalized to other two-dimensional models and possibly higher-order analytic signals.

One method for exploiting the simplicity of the results has been described; perhaps the local wavenumber has other properties and significance we have not yet realized.

Conclusion

Automatic estimation of the location and depth to a magnetic source can be performed quickly and easily with the improved source parameter imaging method. The estimates are independent of an assumed two-dimensional model, the orientation and strength of the earth's magnetic field, and of the dip and susceptibility contrast of the source. The geometric structure of the source can also be determined from the SPI structural index.

The method does assume that the sources are two-dimensional. In practice, we find that when the magnetic contours are approximately parallel, the assumption of

two-dimensionality is reasonable, and good depth and structural index estimations can be obtained.

The estimates of depth and model type obtained from processing the synthetic data are consistent with the known source parameters. Processing of the field example allows easy determination of the depth to the structures in the basement (5 km). These structures are consistent with the known geology, being 300 m below the basement/sediment interface (4.7 km). The lack of significant variation in the interpreted depth around the edges of the body is used to infer that the top of the body is relatively flat, and the value of the SPI structural index allows us to infer that the body is effectively a thin sheet.

In sedimentary basins, where the depth to the basement is not known, the model-independent local wavenumber can be used to obtain an upper estimate of the basement depth.

The images presented can be interpreted easily by an interpreter familiar with the local geology and the current exploration concepts.

Acknowledgements

We thank Dave Daggar, who kindly generated the synthetic model data for Fig. 2, and Alan Reid, for helpful suggestions. Source Parameter Imaging, SPI and iSPI are trademarks of Geoterrex-Dighem.

References

Atchuta Rao D., Ram Babu H.V. and Sanker Narayan P.V. 1981. Interpretation of magnetic anomalies due to dikes: The complex gradient method. *Geophysics* **46**, 1572–1578.

Hartman R.R., Teskey D.J. and Friedberg J.L. 1971. A system for rapid digital aeromagnetic interpretation. *Geophysics* **36**, 891–918.

Hsu S.-K., Sibuet J.-C. and Shyu C.-T. 1996. High-resolution detection of geologic boundaries from potential-field anomalies: An enhanced analytic signal technique. *Geophysics* **61**, 373–386.

Jain S. 1976. An automatic method of direct interpretation of magnetic profiles. *Geophysics* **41**, 531–541.

MacLeod I.N., Jones K. and Dai T.-F. 1993. 3-D analytic signal in the interpretation of total magnetic field data at low magnetic latitudes. *Exploration Geophysics* **24**, 679–688.

Murthy K.S.R. and Mishra D.C. 1980. Fourier transform of the general expression for the magnetic anomaly due to a long horizontal cylinder. *Geophysics* **45**, 1091–1093.

Nabighian M.N. 1972. The analytic signal of two-dimensional magnetic bodies with polygonal cross-section: its properties and use for automated anomaly interpretation. *Geophysics* **37**, 507–517.

Naudy H. 1971. Automatic determination of depth on aeromagnetic profiles. *Geophysics* **36**, 712–722.

Neil C. 1990. *A computer program to interpret automatically potential field data using Euler's equation of inhomogeneity.* MSc thesis, University of Leeds.

Neil C., Whaler K.A. and Reid A.B. 1991. Extensions to Euler's method for three-dimensional potential field interpretation. 53rd EAEG meeting, Florence, Italy, Expanded Abstracts, 416–417.

Reford M.S. 1964. Magnetic anomalies over thin sheets. *Geophysics* **29**, 532–536.

Reid A.B. 1995. Euler deconvolution: Past, present, and future – A review. 65th SEG meeting, Houston, Expanded Abstracts, 272–273.

Reid A.B., Allsop J.M., Granser H., Millet A.J. and Somerton I.W. 1990. Magnetic interpretation in three dimensions using Euler deconvolution. *Geophysics* **55**, 80–91.

Roest W.R., Verhoef J. and Pilkington M. 1992. Magnetic interpretation using the 3-D analytic signal. *Geophysics* **57**, 116–125.

Thompson D.T. 1982. EULDPH: A new technique for making computer-assisted depth estimates from magnetic data. *Geophysics* **47**, 31–37.

Thurston J.B. and Brown R.J. 1994. Automated source edge location with a new variable pass-band horizontal-gradient operator. *Geophysics* **59**, 546–554.

Thurston J.B. and Smith R.S. 1997. Automatic conversion of magnetic data to depth, dip, and susceptibility contrast using the SPI^{TM} method. *Geophysics* **62**, 807–813.